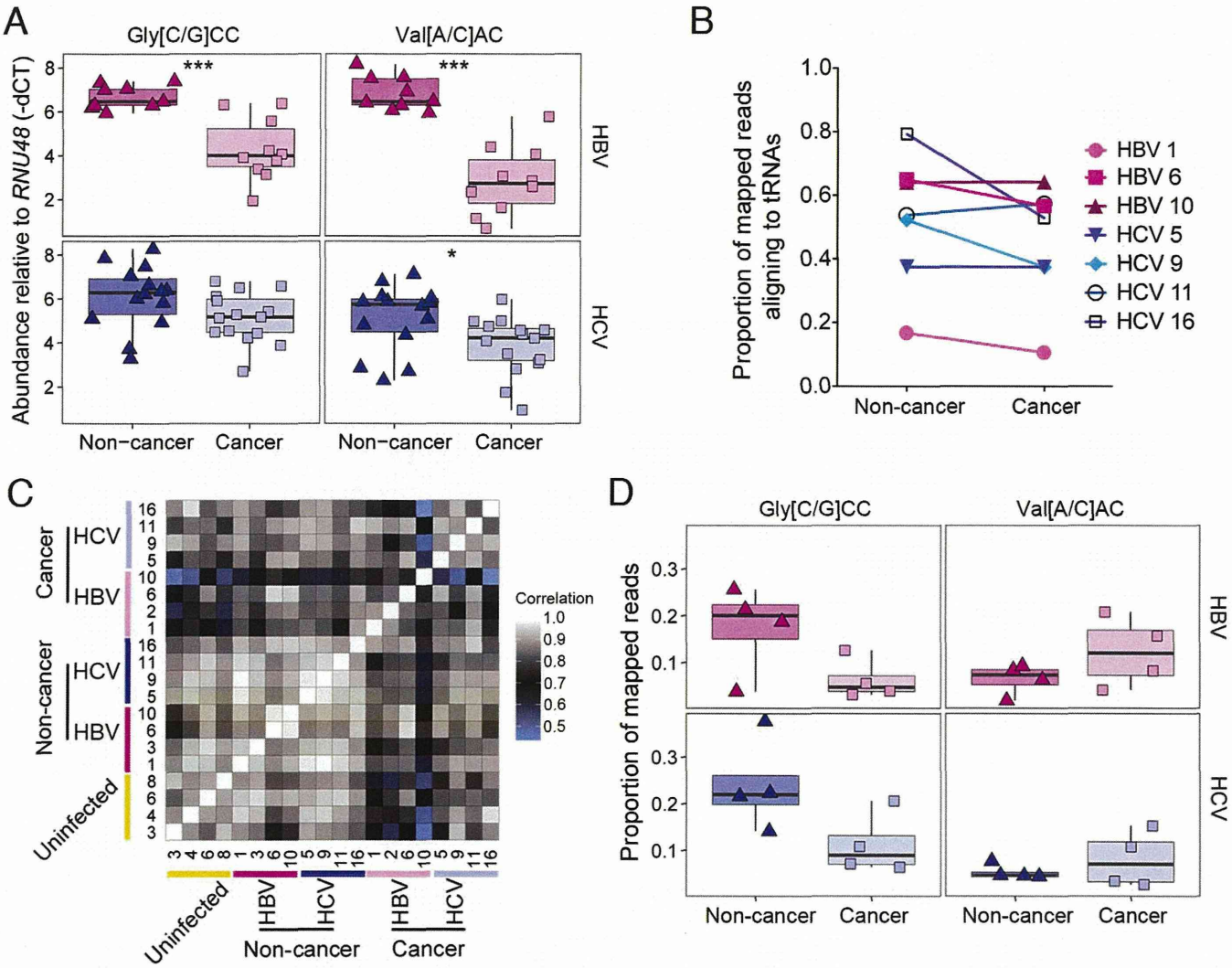

Figure 2 | 5′ tRH abundance in HBV- and HCV-associated hepatocellular carcinoma. (b) Abundance (RT-qPCR) of (left) 5′ tRH^{Gly} (Gly[C/G]CC) and (right) 5′ tRH^{Val} (Val[A/C]AC) in (top) non-malignant (n=9) and cancer tissue (n=10) from HBV-infected subjects, and (bottom) non-malignant (n=14), and cancer tissue (n=15) from HCV-infected subjects. Box and whisker plots are overlaid with data from each sample; whiskers extend to 1.5 * interquartile range. P-values calculated using Mann-Whitney U-test. *P < 0.05; **P < 0.01; ***P < 0.005. (b) Proportion of mapped reads aligning to tRNAs for the paired cancer and non-cancer tissue from subjects with chronic hepatitis B (n=3) and hepatitis C (n=4) (c) Correlation heatmap of tRNA-derived RNA expression profiles determined by small RNA sequencing. The colors of the cells represent Spearman's rank correlation coefficients of the relative levels of the 10 most abundant tRNA-derived RNAs between all pairs of tissue samples sequenced (n=20). (d) Proportion of mapped reads that align to 5′ tRH^{Gly} and 5′ tRH^{Val} in non-malignant and cancer tissue from (top) HBV-infected and (bottom) HCV-infected subjects. "Mapped reads" represents all reads aligning to miRNAs or tRNAs (see Methods).

abundance in seminal exosomes (considered to be immunosuppressive)[28], and roles in facilitating *Trypanosoma cruzi* infection in human cells and altering host gene expression[29].

There is good evidence that the abundance of these small non-coding RNAs increases in response to specific kinds of cellular stress. For example, tRHs are induced in cell culture by the addition of sodium arsenite, exposure to UV, nutrient starvation, hypoxia, hypothermia and heat, but not by exposure to etoposide, γ-radiation, caffeine[30,31]. This strongly suggests that the formation of tRHs is a regulated process, rather than due to general degradation of tRNAs in response to stress. In the nucleus angiogenin is involved in promoting angiogenesis[32] and in the cytoplasm, when not bound to RNH1, it acts as a tRNA-processing RNase[33,34], cleaving tRNAs at the anticodon loop and producing tRHs[30,31]. The cellular localization of angiogenin and its ribonuclease activity depend on the intracellular conditions and are regulated by RNH1[33]. The differences we observed in correlations between ANG expression and tRH abundance in chronic hepatitis B, hepatitis C and associated liver cancer may be a result of differences in angiogenin localization and function in these disease states. Non-tumor and tumor tissues from patients with chronic hepatitis C tend to show more evidence of angiogenesis than the in chronic hepatitis B[35,36]. This could mean that in chronic hepatitis C angiogenin is primarily nuclear, and therefore not exclusively involved in tRH production. Finally, it must also be noted that factors other than ANG may be critical to tRH biogenesis in different cell types or in response to different types of cellular stress. Much more remains to be uncovered about the specific mechanisms that lead to tRH accumulation.

Chronic infections with HBV and HCV typically lead to more severe liver disease in human patients than in the chimpanzee model[37,38]. Disease severity may account for the differences we observed in tRH abundance between liver tissue from human subjects with chronic HCV infection and the chimpanzee samples. Interestingly, however, humans and chimpanzees exhibited similar increases in tRH abundance in chronic hepatitis B, suggesting that

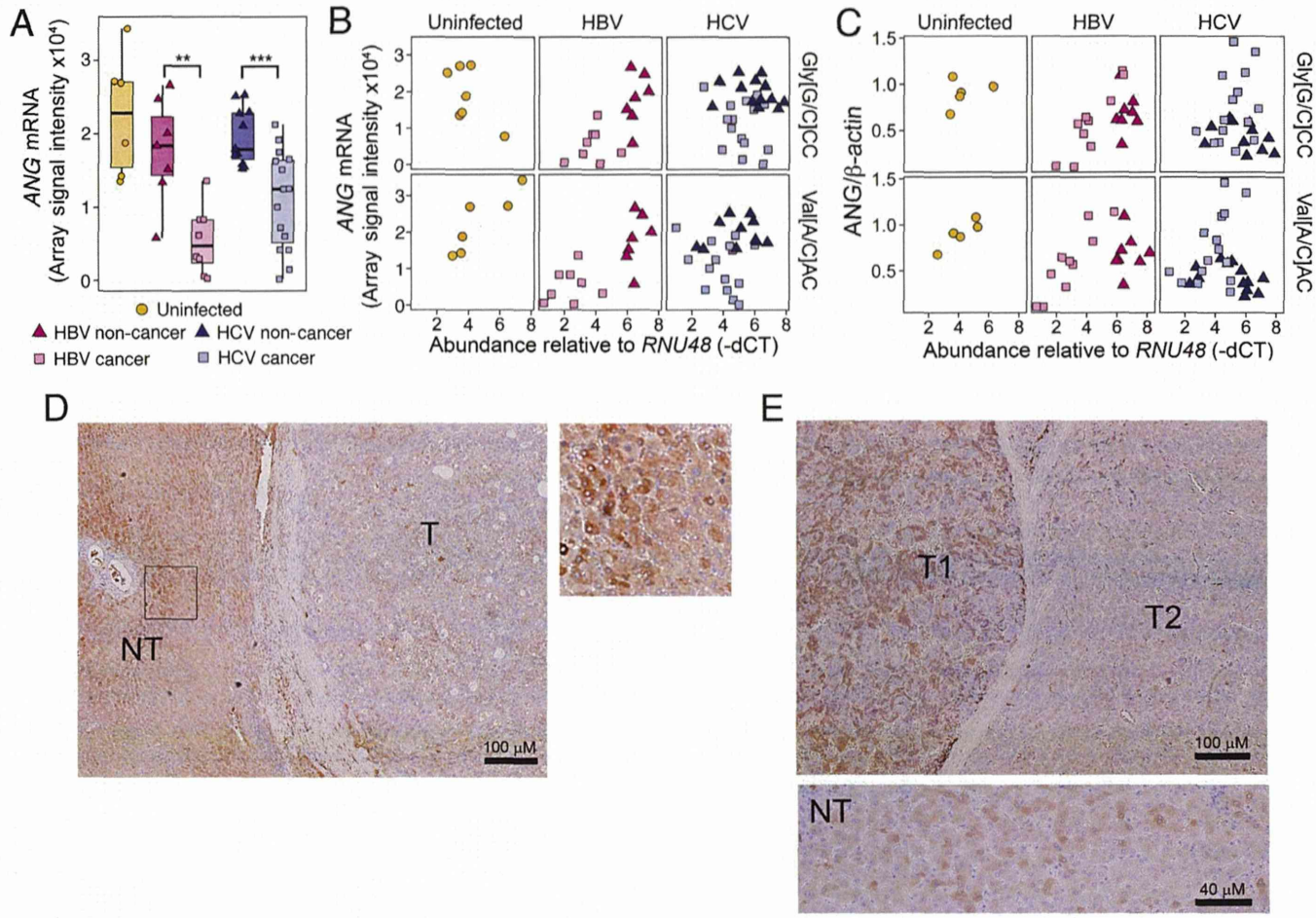

Figure 3 | Angiogenin expression in viral hepatitis and hepatocellular carcinoma. (a) Normalized *ANG* mRNA levels from previously generated liver microarray data[14] from uninfected subjects (n=6), non-malignant (n=7) and liver cancer (n=8) tissue from HBV-infected subjects, and non-malignant (n=11) and cancer tissue (n=15) from HCV-infected subjects. **P < 0.01; ***P < 0.005, calculated by Mann-Whitney U-test. (b) Scatter plot of the levels of 5′ tRHs (RT-qPCR, -dCT normalized to *RNU48*) and *ANG* mRNA (microarray). 5′ tRH^{Gly} ("Gly[C/G]CC"): uninfected subjects (n=7), non-cancer (n=7) and cancer (n=8) liver tissue from chronic hepatitis B subjects, and non-cancer (n=11) and cancer (n=15) liver tissue from chronic hepatitis C subjects; 5′ tRH^{Val}: uninfected subjects (n=6), non-cancer (n=7) and cancer (n=8) liver tissue from chronic hepatitis B subjects, and non-cancer (n=11) and cancer (n=15) liver tissue of chronic hepatitis C subjects. (c) Scatter plot of the levels of 5′ tRHs (RT-qPCR, -dCT normalized to *RNU48*) and ANG protein expression (normalized to β-actin) determined by immunoblot analysis. (d) Immunohistochemistry staining for ANG in formalin-fixed non-tumor (NT) and tumor tissue (T) from HBV-infected subject #10. (Right) Magnified view of non-tumor (NT). (e) ANG staining in adjacent tumor nodules (T1 and T2) and in non-tumor (NT) tissue from HCV-infected subject #7.

there may be a primary HBV-specific mechanism that directly regulates tRH biogenesis.

Our study has some technical limitations. tRNAs are subject to many different chemical modifications[39], several of which could impede library preparation and sequencing. This may have biased which tRNA-derived RNAs we detected. Also, we do not know how tRH abundance varies among the diverse cell types that populate the liver. Given that these small RNAs have not previously been studied in human tissue, we also have little appreciation of what functions these small non-coding RNAs have within the liver. Nonetheless, our finding that the intrahepatic abundance of tRHs is substantially increased in chronic viral infections of the liver and altered in HCC suggest that tRHs may have important, yet to be determined roles in liver disease. Thus, this study may have implications for disease pathogenesis and novel therapeutic strategies.

Methods

The methods were carried out in accordance with the approved guidelines.

Human subjects. Written informed consent was obtained from all human subjects. Ethics approval was obtained from the Ethics Committee for Human Genome/Gene Analysis Research at Kanazawa University Graduate School of Medical Science.

Chimpanzee liver tissue. The chimpanzee samples used in this study were archived from previous studies and were collected prior to December 15, 2011. Chimpanzees were housed and cared for at the Southwest National Primate Research Center (SNPRC) of the Texas Biomedical Research Institute. The animals were cared for in accordance with the Guide for the Care and Use of Laboratory Animals, and all protocols were approved by the Institutional Animal Care and Use Committee. SNPRC is accredited by the Association for Assessment and Accreditation of Laboratory Animal Care (AAALAC) International. SNPRC operates in accordance with the NIH and U.S. Department of Agriculture guidelines and the Animal Welfare Act. Animals were sedated for all procedures. Animals are group-housed with indoor and outdoor access and an environmental enrichment program is provided by a staff of behavioral scientists.

Small RNA-sequencing. RNA was isolated as described previously[14]. RNA purity was assessed with Nanodrop 2000 (Thermo Scientific) and integrity was determined with an Agilent 2100 Bioanalyzer (Agilent). RNA integrity and sequencing quality were comparable for all specimens (Supplemental Table 2–4). Small RNA libraries were generated using Illumina TruSeq Small RNA Sample Preparation Kit (Illumina, San Diego, CA). Sequencing was performed on Illumina HiSeq 2000 platform. Bioinformatic analysis: Sequencing reads were trimmed using Cutadapt (parameters O -10 e 0.1) and were further analyzed in two different ways: (i) Mapped trimmed reads allowing no mismatches to all tRNA sequences (except pseudo-tRNAs and undefined tRNAs) downloaded from GtRNAdb[16] (Figure 1b,c; Figure 2c,d; Supplemental Figure 1,2,4,7); (ii) Mapped trimmed reads to genomic regions spanning annotated miRNA s[40] (+/− 20 nts) and tRNA sequences (+/− 40 nts) using Bowtie 0.12.7[41] allowing for no mismatches. Next, reads that did not map

without mismatches were aligned to the same regions using SHRiMP2.2.2[42]. SHRiMP2.2.2 seeds were set based on the length of the read allowing 1 mismatch anywhere in the body and up to 3 mismatches at the 3′ end of the read (based on the length of the read). (Figure 1a right, Figure 2b, Supplemental Figure 7, Supplemental Table 4). Small RNA-sequencing data was deposited on GEO (GSE57381).

AGO2-RNA Co-immunoprecipitation. FT3-7 cells were grown in Dulbecco's modified Eagle's medium (DMEM, Life Technologies) and supplemented with 10% fetal calf serum and 2 mM GlutaMAX (Life Technologies, Carlsbad, CA). Cells were cultured in a humidified incubator at 37°C and 5% CO_2. Three technical replicates of 1×10^7 FT3-7 cells were harvested in lysis buffer [150 mM KCl, 25 mM Tris-HCl (pH 7.4), 5 mM EDTA, 1% Triton X-100, 5 mM DTT, Complete protease inhibitor mixture (Roche), and 100 U/mL RNaseOUT (Life Technologies)]. Lysates were centrifuged for 30 min at 17,000 × g at 4°C and filtered through a 0.22-um filter. Filtrates were incubated with anti-human AGO2 mAb (RN003M, MBL International, Woborn, MA) or isotype control IgG (Abcam, Cambridge, England) at 4°C for 2 h, followed by addition of 30 μL of Protein G Sepharose (GE Healthcare) for 1 h. The Sepaharose beads were washed three times in lysis buffer and RNA extracted using the miRNeasy Mini Kit (Qiagen, Hilden, Germany).

Small RNA real time quantitative PCR (RT-qPCR). Complementary DNA (cDNA) was synthesized using TaqMan MicroRNA Reverse Transcription Kit (Life Technologies) according to the manufacturer's instructions. Real time PCR amplification was performed using TaqMan Universal Master Mix (Life Technologies) on the Bio-Rad CFX96 real time PCR detection system. *U6*, miR-24, let-7a, let-7f, *RNU48*, and *RNU66* were all evaluated as potential housekeeping small RNAs for purposes of normalization. *RNU48* was selected because it was the most consistent across disease groups. RT-qPCR reactions for human samples were performed in triplicate. RT-qPCR reactions for chimpanzee samples were performed in duplicate. The following TaqMan assays were purchased from Life Technologies: miR-122 (product number 4427975; 002245) and *RNU48* or *SNORD48* (product number 4427975; 001006). Primers for the custom TaqMan assays (5′ tRH^{Gly} and 5′ tRH^{Val}) were designed using 5′-GCAUUGGUGGUUCAGUGGUAGAAU-UCUCGCCU-3′ for 5′ tRH^{Gly} and 5′-GUUUCCGUAGUGUAGUGGUUAUCAC-GUUCGCCU-3′ for 5′ tRH^{Val}.

Metabolic Radiolabeling and Measurement of Nascent Protein Synthesis. Huh7 cells were seeded onto the wells of 6-well cell culture plates at a density of 2×10^5 cells/well and incubated overnight to allow cell attachment. Cells were transfected with 50 nM and 100 nM of 5′ tRH^{Gly} (5′-GCAUUGGUGGUUCAGUGGUAGAAU-UCUCGCCU-3′), 5′ tRH^{Val} (5′-GUUUCCGUAGUGUAGUGGUUAUCACGUU-CGCCU-3′), or scramble (5′-GCAUUCACUUGGAUAGUAAAUCCAAGC-UGAA-3′)[21] (all from Integrated DNA Technologies, Coralville, IA) oligonucleotide after replacing cell culture medium with methionine- and cysteine-deficient DMEM (Life Technologies) and cultured for further 12 hrs. Cells were then metabolically radiolabeled for 12 hrs with 200 μCi/well of Express Protein Labeling Mix containing [^{35}S]methionine and [^{35}S]cysteine (PerkinElmer, Waltham, MA) in the presence or absence of 50 μg/ml puromycin and lysed with lysis buffer (20 mM Tris-HCl [pH 7.4] containing 150 mM NaCl, 1% Triton X-100, 0.05% SDS, and 10% glycerol) supplemented with 50 mM NaF, 5 mM Na_3VO_4, and a protease inhibitor cocktail (Complete; Roche, Mannheim, Germany). The protein concentration of cell lysates was determined by the Bio-Rad Protein Assay (Bio-Rad), and 10 μg (total protein) of cell lysates was subjected to SDS-PAGE followed by staining gels with the Sypro Ruby Protein Gel Stain (Bio-Rad, Hercules, CA) and autoradiography.

Immunohistochemistry (IHC). Staining was performed by immunoperoxidase technique with an Envision kit (DAKO Japan). Primary antibodies used were against β-actin (Cell signaling technology, #4967, Beverly, MA) and Human Angiogenin Affinity Purified Polyclonal Ab (R and D Systems, AF265, Minneapolis, MN).

1. Arzumanyan, A., Reis, H. M. & Feitelson, M. A. Pathogenic mechanisms in HBV- and HCV-associated hepatocellular carcinoma. *Nat Rev Cancer* **13**, 123–135 (2013).
2. Perz, J. F., Armstrong, G. L., Farrington, L. A., Hutin, Y. J. & Bell, B. P. The contributions of hepatitis B virus and hepatitis C virus infections to cirrhosis and primary liver cancer worldwide. *J Hepatol* **45**, 529–538 (2006).
3. Hou, W. & Bonkovsky, H. L. Non-coding RNAs in hepatitis C-induced hepatocellular carcinoma: dysregulation and implications for early detection, diagnosis and therapy. *World J Gastroenterol* **19**, 7836–7845 (2013).
4. Xu, X. *et al.* Hepatitis B virus X protein represses miRNA-148a to enhance tumorigenesis. *J Clin Invest* **123**, 630–645 (2013).
5. Chen, Y. *et al.* HCV-induced miR-21 contributes to evasion of host immune system by targeting MyD88 and IRAK1. *PLoS Pathog* **9**, e1003248 (2013).
6. Jopling, C. L., Yi, M., Lancaster, A. M., Lemon, S. M. & Sarnow, P. Modulation of hepatitis C virus RNA abundance by a liver-specific MicroRNA. *Science* **309**, 1577–1581 (2005).
7. Shimakami, T. *et al.* Stabilization of hepatitis C virus RNA by an Ago2-miR-122 complex. *Proc Natl Acad Sci U S A* **109**, 941–946 (2012).
8. Janssen, H. L. *et al.* Treatment of HCV Infection by Targeting MicroRNA. *N Engl J Med* **368**, 1685–1694 (2013).
9. Garcia-Silva, M. R., Cabrera-Cabrera, F. & Güida, M. C. Hints of tRNA-Derived Small RNAs Role in RNA Silencing Mechanisms. *Genes* **3**, 603–614 (2012).
10. Wang, Q. *et al.* Identification and functional characterization of tRNA-derived RNA fragments (tRFs) in respiratory syncytial virus infection. *Mol Ther* **21**, 368–379 (2013).
11. Gong, B. *et al.* Compartmentalized, functional role of angiogenin during spotted fever group rickettsia-induced endothelial barrier dysfunction: evidence of possible mediation by host tRNA-derived small noncoding RNAs. *BMC Infect Dis* **13**, 285 (2013).
12. Saikia, M. *et al.* Angiogenin-Cleaved tRNA Halves Interact with Cytochrome c Protecting Cells from Apoptosis during Osmotic Stress. *Mol Cell Biol* **34**, 2450–63 (2014).
13. Hou, J. *et al.* Identification of miRNomes in human liver and hepatocellular carcinoma reveals miR-199a/b-3p as therapeutic target for hepatocellular carcinoma. *Cancer Cell* **2**, 232–243 (2011).
14. Spaniel, C., Honda, M., Selitsky, S. R. & Yamane, D. microRNA-122 abundance in hepatocellular carcinoma and non-tumor liver tissue from Japanese patients with persistent HCV versus HBV infection. *PloS One* **8**, e76867 (2013).
15. Bartel, D. P. MicroRNAs: target recognition and regulatory functions. *Cell* **136**, 215–233 (2009).
16. Chan, P. P. & Lowe, T. M. GtRNAdb: a database of transfer RNA genes detected in genomic sequence. *Nucleic Acids Res* **37**, D93–97 (2009).
17. Kozomara, A. & Griffiths-Jones, S. miRBase: annotating high confidence microRNAs using deep sequencing data. *Nucleic Acids Res* **42**, D68–73 (2014).
18. Lanford, R. E., Lemon, S. M. & Walker, C. in *Hepatitis C Antiviral Drug Discovery & Development* (eds He, Y. & Tan, T.) 99–132 (Horizons Scientific Press, 2011).
19. Asabe, S. *et al.* The size of the viral inoculum contributes to the outcome of hepatitis B virus infection. *J Virol* **83**, 9652–9662 (2009).
20. Fu, H. *et al.* Stress induces tRNA cleavage by angiogenin in mammalian cells. *FEBS Lett* **583**, 437–442 (2009).
21. Yamasaki, S., Ivanov, P., Hu, G.-F. & Anderson, P. Angiogenin cleaves tRNA and promotes stress-induced translational repression. *J Cell Biol* **185**, 35–42 (2009).
22. Wang, Q. *et al.* Identification and functional characterization of tRNA-derived RNA fragments (tRFs) in respiratory syncytial virus infection. *Mol Ther* **21**, 368–379 (2013).
23. Gong, B. *et al.* Compartmentalized, functional role of angiogenin during spotted fever group rickettsia-induced endothelial barrier dysfunction: evidence of possible mediation by host tRNA-derived small noncoding RNAs. *BMC Infect Dis* **13**, 285 (2013).
24. Mishima, E. *et al.* Conformational Change in Transfer RNA Is an Early Indicator of Acute Cellular Damage. *J Am Soc Nephrol* **25**, 2316–26 (2014).
25. Ivanov, P., Emara, M. M., Villen, J., Gygi, S. P. & Anderson, P. Angiogenin-induced tRNA fragments inhibit translation initiation. *Mol Cell* **43**, 613–623 (2011).
26. Emara, M. M. *et al.* Angiogenin-induced tRNA-derived stress-induced RNAs promote stress-induced stress granule assembly. *J Biol Chem* **285**, 10959–10968 (2010).
27. Dhahbi, J. M. *et al.* 5′ tRNA halves are present as abundant complexes in serum, concentrated in blood cells, and modulated by aging and calorie restriction. *BMC Genomics* **14**, 298 (2013).
28. Vojtech, L. *et al.* Exosomes in human semen carry a distinctive repertoire of small non-coding RNAs with potential regulatory functions. *Nucleic Acids Res* **42**, 7290–7304 (2014).
29. Garcia-Silva, M. R. *et al.* Gene Expression Changes Induced by Trypanosoma cruzi Shed Microvesicles in Mammalian Host Cells: Relevance of tRNA-Derived Halves. *Biomed Res Int* **2014**, 305239 (2014).
30. Fu, H. *et al.* Stress induces tRNA cleavage by angiogenin in mammalian cells. *FEBS Lett* **583**, 437–442 (2009).
31. Yamasaki, S., Ivanov, P., Hu, G.-F. & Anderson, P. Angiogenin cleaves tRNA and promotes stress-induced translational repression. *J Biol Chem* **185**, 35–42 (2009).
32. Gao, X. & Xu, Z. Mechanisms of action of angiogenin. *Acta Biochim Biophys Sin (Shanghai)* **40**, 619–624 (2008).
33. Pizzo, E. *et al.* Ribonuclease/angiogenin inhibitor 1 regulates stress-induced subcellular localization of angiogenin to control growth and survival. *J Cell Sci* **126**, 4308–4319 (2013).
34. Saxena, S. K., Rybak, S. M., Davey, R. T., Youle, R. J. & Ackerman, E. J. Angiogenin is a cytotoxic, tRNA-specific ribonuclease in the RNase A superfamily. *J Biol Chem* **267**, 21982–21986 (1992).
35. Mazzanti, R. *et al.* Chronic viral hepatitis induced by hepatitis C but not hepatitis B virus infection correlates with increased liver angiogenesis. *Hepatology* **25**, 229–234 (1997).
36. Messerini, L., Novelli, L. & Comin, C. E. Microvessel density and clinicopathological characteristics in hepatitis C virus and hepatitis B virus related hepatocellular carcinoma. *J Clin Pathol* **57**, 867–871 (2004).
37. Walker, C. M. Comparative features of hepatitis C virus infection in humans and chimpanzees. *Springer Semin Immunopathol* **19**, 85–98 (1997).
38. Mason, W. S. *et al.* Detection of clonally expanded hepatocytes in chimpanzees with chronic hepatitis B virus infection. *J Virol* **83**, 8396–8408 (2009).
39. Jackman, J. E. & Alfonzo, J. D. Transfer RNA modifications: nature's combinatorial chemistry playground. *Wiley Interdisciplin Rev RNA* **4**, 35–48 (2013).

40. Kozomara, A. & Griffiths-Jones, S. miRBase: annotating high confidence microRNAs using deep sequencing data. *Nucleic Acids Res* **42**, D68–73 (2014).
41. Langmead, B., Trapnell, C., Pop, M. & Salzberg, S. L. Ultrafast and memory-efficient alignment of short DNA sequences to the human genome. *Genome Biol* **10**, R25 (2009).
42. David, M., Dzamba, M., Lister, D., Ilie, L. & Brudno, M. SHRiMP2: sensitive yet practical short read mapping. *Bioinformatics* **27**, 1011–2 (2011).
43. Larkin, M. A., Blackshields, G., Brown, N. P. & Chenna, R. Clustal W and Clustal X version 2.0. *Bioinformatics* **23**, 2947–2948 (2007).

Acknowledgments

This work was supported by grants from the National Institutes of Health: R00-DK091318 (P.S.); R01-AI095690 and R01-CA164029 (S.M.L); T32-GM067553 and T32-AI007419 (S.R.S). The Southwest National Primate Research Center is supported by a grant from the NIH Office of Research Infrastructure Programs/OD P51 OD011133), and by Research Facilities Improvement Program Grants C06 RR 12087 and C06 RR016228.

Author contributions

The experiments were designed by S.R.S., P.S. and S.M.L. The data were analyzed by S.R.S., J.B., T. Shirasaki, M.H., P.S. and S.M.L. Experiments were performed by S.R.S., D.Y., T.M., E.E.F., B.G. and T. Shirasaki. M.H., T. Shimakami, S.K., R.E.L., S.M.L. and P.S. contributed resources. The manuscript was written by S.R.S., P.S. and S.M.L.

Additional information

Supplementary information accompanies this paper at http://www.nature.com/scientificreports

Competing financial interests: The authors declare no competing financial interests.

How to cite this article: Selitsky, S.R. *et al.* Small tRNA-derived RNAs are increased and more abundant than microRNAs in chronic hepatitis B and C. *Sci. Rep.* **5**, 7675; DOI:10.1038/srep07675 (2015).

Liver INTERNATIONAL

Liver International ISSN 1478-3223

NAFLD & NASH

Characteristics of hepatic fatty acid compositions in patients with nonalcoholic steatohepatitis

Kazutoshi Yamada[1], Eishiro Mizukoshi[1], Hajime Sunagozaka[1], Kuniaki Arai[1], Tatsuya Yamashita[1], Yumie Takeshita[2], Hirofumi Misu[2], Toshinari Takamura[2], Seiko Kitamura[3], Yoh Zen[3], Yasuni Nakanuma[4], Masao Honda[1] and Shuichi Kaneko[1]

1 Department of Gastroenterology, Graduate School of Medicine, Kanazawa University, Kanazawa, Japan
2 Department of Disease Control and Homeostasis, Graduate School of Medicine, Kanazawa University, Kanazawa, Japan
3 Division of Pathology, Kanazawa University Hospital, Kanazawa, Japan
4 Department of Human Pathology, Graduate School of Medicine, Kanazawa University, Kanazawa, Japan

Keywords
fatty acid metabolism – insulin resistance – palmitic acid – toxic lipid

Abbreviations
ACC, acetyl-CoA carboxylase; BMI, body mass index; ELOVL6, elongation of long-chain fatty acids family member 6; FAS, fatty acid synthase; HOMA-IR, homoeostasis model assessments of insulin resistance; NAFLD, nonalcoholic fatty liver disease; NASH, nonalcoholic steatohepatitis; NAS, NAFLD activity score; PPAR, peroxisome proliferator-activated receptor; QUICKI, Quantitative Insulin Sensitivity Check Index; SCD, stearoyl-CoA desaturase; SREBP-1c, sterol regulatory element-binding protein-1c; SS, simple steatosis; T-CHO, total cholesterol; TG, triglyceride.

Correspondence
Shuichi Kaneko, Department of Gastroenterology, Graduate School of Medicine, Kanazawa University, Kanazawa, Ishikawa 920-8641, Japan
Tel: +81 76 265 2230
Fax: +81 76 234 4250
e-mail: skaneko@m-kanazawa.jp

Received 9 January 2014
Accepted 3 September 2014

DOI:10.1111/liv.12685
Liver Int. 2015; 35: 582–590

Abstract

Background & Aims: Nonalcoholic fatty liver disease (NAFLD) is closely related to insulin resistance and lipid metabolism. Recent studies have suggested that the quality of fat accumulated in the liver is associated with the development of nonalcoholic steatohepatitis (NASH). In this study, we investigated the fatty acid composition in liver tissue and its association with the pathology in NAFLD patients. *Methods:* One hundred and three patients diagnosed with NAFLD [simple steatosis (SS): 63, NASH: 40] were examined and their hepatic fatty acids were measured using gas chromatography. In addition, relationships between the composition and composition ratios of various fatty acids and patient backgrounds, laboratory test values, histology of the liver, and expression of fat metabolism-related enzymes were investigated. *Results:* The C16:1n7 content, the C16:1n7/C16:0 and C18:1n9/C18:0 ratios were increased and the C18:0/C16:0 ratio was decreased in the NASH group. The C18:0/C16:0 and C18:1n9/C18:0 ratios were associated with the steatosis score in liver tissue, and the C16:1n7/C16:0 ratio was associated with the lobular inflammation score. The expressions levels of genes: SCD1, ELOVL6, SREBP1c, FAS and PPARγ were enhanced in the NASH group. In multivariate analysis, the C18:0/C16:0 ratio was the most important factor that was correlated with the steatosis score. In contrast, the C16:1n7/C16:0 ratio was correlated with lobular inflammation. *Conclusion:* The fatty acid composition in liver tissue and expression of genes related to fatty acid metabolism were different between the SS and NASH groups, suggesting that the acceleration of fatty acid metabolism is deeply involved in pathogenesis of NASH.

The number of patients with nonalcoholic fatty liver disease (NAFLD) has increased in Western countries and Asia, and the increase in obese people and changes in dietary life has become a major health issue (1, 2). NAFLD includes simple steatosis (SS) with a favourable prognosis and nonalcoholic steatohepatitis (NASH). NASH is considered to develop when an exacerbating factor is added to fat deposition in liver tissue, with oxidative stress, inflammatory cytokines and iron-related factor being attributed as causes of NASH (3–5). However, the detailed developmental mechanism for NASH has not been fully elucidated and no evidence-based treatment method has been established, although several drugs have been suggested to be effective (6–8). The prognosis is poor once the condition has progressed to NASH, and the incidence of liver-related death significantly increases with the progression to hepatic cirrhosis. Therefore, identifying factors that con-

tribute to the progression of SS to NASH is vitally important and a treatment method needs to be established to prevent its progression.

Previous studies have clarified that insulin resistance is closely involved in the development of NAFLD (9–11). On the other hand, it has recently been reported that the composition of fatty acids in liver tissue and the expression level of elongation of long-chain fatty acids family member 6 (ELOVL6), which regulates their composition, are factors determining insulin resistance (12), and reducing the activity of fatty acid desaturase, stearoyl-CoA desaturase 1 (SCD1), exacerbates hepatocellular disorders and liver tissue fibrosis (13). These reports have suggested an association between the development of NAFLD or NASH and the amount and composition ratios of fatty acids accumulated in the liver and the expression of enzymes regulating them. In a previous report on liver tissue fatty acids in NAFLD patients, the fatty acid composition was different from that in healthy subjects; however, the number of subjects was small and how these changes were associated with the clinical characteristics of NAFLD was not clarified (14).

Thus, in this study, we measured the fatty acid contents of liver tissue in 103 NAFLD patients, clarified the characteristics of the composition and composition ratio of these fatty acids, and investigated their association with the disease state and pathological changes. In addition, we analysed the gene expression of enzymes involved in fatty acid synthesis and degradation, which influence changes in the liver tissue fatty acid composition, and clarified their roles in the pathogenesis of NAFLD.

Materials and methods

Patients and laboratory testing

The subjects in this study were 103 patients diagnosed with NAFLD based on pathological examinations of liver tissue collected by ultrasound-guided percutaneous liver biopsies at our institution between December 1998 and September 2010. All patients were hepatitis B surface antigen (HBsAg) and hepatitis C virus antibody negative, and the volume of alcohol consumption per day was less than 20 g. A pathological evaluation was independently performed by two pathologists, and diagnoses were made based on Matteoni's classification (15). Types 1 and 2 of this classification were defined as SS and types 3 and 4 were defined as NASH (SS: 63 patients, NASH: 40 patients). In all patients, three items of the NAFLD activity score (NAS; steatosis, lobular inflammation and hepatocellular ballooning) and fibrosis were also scored (16). In addition, 18 patients who underwent hepatectomy or autopsy for other diseases with no fibrosis or fatty changes on pathological examination of the liver or other chronic liver diseases were included as controls. The first biopsy sample was used in patients who underwent liver biopsies multiple times. All patients gave written informed consent to participate in the study in accordance with the Helsinki Declaration and this study was approved by the Regional Ethics Committee (Medical Ethics Committee of Kanazawa University, no. 829).

The blood test findings of patients whose blood was collected in a fasting state on admission for liver biopsy were adopted.

Insulin resistance was evaluated based on homoeostasis model assessments of insulin resistance (HOMA-IR) [fasting serum insulin (μU/ml) × fasting plasma glucose (mg/dl)/405] and the Quantitative Insulin Sensitivity Check Index (QUICKI) [1/log (fasting serum insulin (μU/ml) × fasting plasma glucose (mg/dl)/405] calculated from fasting-state blood glucose and insulin levels. In some patients (20 SS and 15 NASH patients), insulin resistance was also evaluated by performing the hyperinsulinaemic–euglycaemic clamp (17).

Fatty acid extraction

Liver specimens collected by percutaneous liver biopsy or hepatectomy were used. The wet weight of the liver specimen was measured, and fatty acids were extracted as follows: The liver specimen was placed in KOH methanol solution, combined with 100 μl of pentadecanoic acid methanol solution as an internal reference, and saponified by heating at 100°C for 30 min. After acidifying the solution with 1 N aqueous hydrochloric acid solution, fatty acids were extracted by adding hexane as a solvent, followed by methyl esterification using 14% BF3 methanol solution (P/N1022-12002, GL Sciences, Tokyo, Japan).

Measurement and analysis of liver tissue fatty acids

Extracted fatty acids were identified and quantified by gas chromatography using a Shimadzu, Kyoto, Japan Gas Chromatograph GC-2014AF/SPL and Rtx-2330 column. Chromatographs were analysed using GC solution version 2.3. (Shimadzu Corporation, Kyoto, Japan) The external reference method was employed for the identification and quantitative analysis of fatty acids using TM37Component FAME Mix 47885-U of Supelco (Sigma–Aldrich, St. Louis, MO, USA) as a reference solution. The liver tissue fatty acid content was quantified as an amount per 1 mg of wet liver tissue, and differences in the fatty acid content and composition ratio among the Control, SS and NASH groups were investigated. In this study, n-6 fatty acids were calculated by the sum of C18n2n6, 20:3n6 and 20:4n6, while n-3 fatty acids were calculated by the sum of C18:3n3 and C22:6n3. In addition, the association between physical and blood data and the pathological findings of patients with fatty acids were evaluated. To investigate the association of fatty acid-synthesizing enzymes, the substrate: product fatty acid ratio was determined, and differences among the groups and in the pathological characteristics were evaluated.

Quantitative real-time detection-PCR

We performed quantitative real-time detection (RTD)-PCR using TaqMan Universal Master Mix (PE Applied Biosystems, Foster City, CA, USA). Primer pairs and probes for SCD, ELOVL6, SREBF1, FASN, ACACA, PPARA, PPARG and GAPDH were obtained from the TaqMan assay reagent library. Total RNA was isolated from liver tissue samples using an RNA extraction kit (Micro RNA Extraction Kit; Stratagene, La Jolla, CA, USA). We reverse-transcribed 1 μg of isolated RNA to cDNA using SuperScript® II RT (Invitrogen, Carlsbad, CA, USA) according to the manufacturer's instructions, and the resultant cDNA was amplified with appropriate TaqMan assay reagents as previously described (18).

Statistical analysis

Data are expressed as the mean ± SEM. Differences in the clinical features and amount of fatty acids among the three groups consisting of controls, patients with SS and patients with NASH were analysed for significance by Mann–Whitney's *U*-test, Spearman's rank correlation, and single and multiple regression analysis. A level of $P < 0.05$ was considered significant.

Table 1. Characteristics of the study population

Variable	Control (n = 18)	SS (n = 63)	NASH (n = 40)
Gender M/F	10/8	37/26	19/21
Age (years)	62.8 ± 3.9	46.1 ± 1.9*	52.2 ± 2.7*
Height (cm)	160.1 ± 2.5	162.2 ± 1.3	160.5 ± 1.6
Weight (kg)	53.7 ± 2.3	75.6 ± 2.6*	77.0 ± 2.9*
BMI (kg/m²)	20.9 ± 0.7	28.7 ± 0.8*	29.7 ± 0.8*
AST (IU/L)	32.9 ± 7.2	35.3 ± 5.7	56.9 ± 4.6*,†
ALT (IU/L)	32.2 ± 5.8	58.4 ± 11.6*	82.0 ± 7.3*,†
PLT (×10⁴/mm³)	22.6 ± 1.8	24.0 ± 0.9	20.3 ± 1.1
Total Protein (g/dl)	6.5 ± 0.3	7.0 ± 0.1*	7.1 ± 0.1*
Albumin (g/dl)	3.3 ± 0.2	4.4 ± 0.1*	4.21 ± 0.1*,†
PT (%)	77.9 ± 4.2	97.8 ± 1.7*	97.2 ± 2.7*
HbA1c (%)	5.8 ± 0.3	7.1 ± 0.2*	7.1 ± 0.3*
HOMA-IR	–	3.8 ± 0.5	7.2 ± 1.3*,†
QUICKI	–	0.33 ± 0.0	0.30 ± 0.0†
GIR (mg/kg/min)	–	5.9 ± 0.6	4.3 ± 0.3†
Total cholesterol (mg/dl)	165.5 ± 11.7	201.2 ± 5.2*	193.9 ± 5.7*
Triglycerides (mg/dl)	90.1 ± 9.5	135.4 ± 9.3*	153.6 ± 15.2*
HDL cholesterol (mg/dl)	43.2 ± 4.2	46.1 ± 1.2	49.0 ± 2.2
LDL cholesterol (mg/dl)	107.9 ± 10.6	127.8 ± 4.9	115.6 ± 5.1

The data are expressed as the mean ± SEM.
ALT, alanine aminotransferase; AST, aspartate aminotransferase; GIR, glucose infusion rate.
*$P < 0.05$ vs. the control.
†$P < 0.05$ vs. SS.

Results

Patient profiles

The backgrounds of patients in the Control, SS and NASH groups are shown in Table 1. The mean age of the patients was 50.6 years, and the male: female ratio was 66:55. No significant difference was observed in the use of medications for dyslipidaemia and diabetes between the SS and NASH groups. The body mass index (BMI), haemoglobin A1c (HbA1c) value, and total cholesterol (T-CHO) and triglyceride (TG) levels were significantly higher in the SS and NASH groups than in the Control group. Aspartate aminotransferase and alanine

Table 2. Histopathological findings of livers in the study population

	SS	NASH	*P*-value
Fibrosis (0/1/2/3/4)	7/52/4/0/0	1/15/11/7/6	< 0.01
Steatosis (0/1/2/3)	0/30/24/9	0/10/15/15	< 0.01
Lobular inflammation (0/1/2/3)	6/34/23/0	0/8/26/6	< 0.01
Hepatocellular ballooning (0/1/2)	41/21/1	1/17/22	< 0.01

Table 3. Fatty acid composition in liver tissue of the study population

	Control (n = 18)	SS (n = 63)	NASH (n = 40)
C12:0	0.25 ± 0.10	10.9 ± 2.3*	14.4 ± 3.5*
C14:0	2.4 ± 0.5	36.9 ± 5.1*	67.2 ± 1.4*
C16:0	54.5 ± 6.7	528 ± 80.3*	928 ± 210*
C16:1n7	5.6 ± 1.0	58.3 ± 10.6*	109 ± 23.5*,†
C17:0	3.4 ± 1.8	15.6 ± 2.4*	20.3 ± 3.9*
C18:0	33.6 ± 4.9	162 ± 24.3*	210 ± 40.4*
C18:1n9	36.0 ± 4.8	616 ± 110*	1036 ± 234*
C18:2n6	36.2 ± 3.9	270 ± 46.5*	387 ± 75.7*
C20:1n9	1.0 ± 0.3	18.1 ± 3.3*	24.7 ± 4.4*
C18:3n3	0.4 ± 0.1	6.0 ± 1.0*	9.1 ± 1.9*
C22:1n9	19.1 ± 2.7	56.3 ± 7.8*	57.6 ± 9.5*
C22:2n6	3.08 ± 0.6	10.9 ± 1.5*	10.9 ± 1.5*
C22:6n3	21.7 ± 3.7	54.2 ± 6.8*	51.2 ± 6.8*
C18:0/C16:0 ratio	0.62 ± 0.02	0.35 ± 0.01*	0.27 ± 0.01*,†
C16:1n7/ C16:0 ratio	0.10 ± 0.01	0.10 ± 0.00	0.13 ± 0.01†
C18:1n9/ C18:0 ratio	1.17 ± 0.12	3.43 ± 0.20*	4.22 ± 0.19*,†
n-6/n-3	2.18 ± 0.24	4.21 ± 0.26*	5.25 ± 0.38*,†

The data are expressed as 10^{-4} mg/mg liver, the mean ± SEM.
Lauric acid (C12:0), myristic acid (C14:0), palmitic acid (C16:0), palmitoleic acid (C16:1n7), heptadecanoic acid (C17:0), stearic acid (C18:0), oleic acid (C18:1n9), linoleic acid (C18:2n6), gondoic acid (C20:1n9), α-linolenic acid (C18:3n3), erucic acid (C22:1n9), docosadienoic acid (C22:2n6), docosahexaenoic acid (C22:6n3).
*$P < 0.05$ vs. the control.
†$P < 0.05$ vs. SS.

aminotransferase were significantly higher, and the platelet count and albumin level were significantly lower in the NASH group than in the SS group. HOMA-IR, QUICKI and the glucose infusion rate were significantly different between the groups, with insulin resistance being significantly higher in the NASH group.

The histopathological findings of livers are shown in Table 2. The progression of steatosis, inflammation, hepatocellular disorders and fibrosis was significantly further in the NASH group than in the SS group.

Comparison of the fatty acid content of liver tissue

The fatty acids shown in Table 3 were measured in extracts from liver tissue using gas chromatography. When the fatty acid content per 1 mg of wet liver was compared, various fatty acid contents were significantly higher in the SS and NASH groups than in the control group ($P < 0.05$). In addition, the palmitoleic acid (C16:1n7) content was significantly higher in the NASH group than in the SS group ($P < 0.05$).

Regarding the fatty acid composition ratio, the stearic acid (C18:0)/palmitic acid (C16:0) ratio was significantly lower ($P < 0.01$) and the C16:1n7/C16:0 and oleic acid (C18:1n9)/C18:0 ratios were significantly higher in the NASH group than in the SS group ($P < 0.01$). Differences in the fatty acid composition ratio between the SS and NASH groups were more prominent in men, while no significant difference was noted in premenopausal women (Table S1). The n-6/n-3 ratio was significantly higher in the NASH group than in the SS group ($P < 0.05$). (Table 3)

Fatty acid composition ratio and insulin resistance

The association between the fatty acid composition ratio in liver tissue and insulin resistance was investigated. For the indices of insulin resistance, HOMA-IR and QUICKI calculated from the fasting-state blood glucose and insulin levels were used. Firstly, patients were divided into two groups with (>2.5) and without (≦2.5) insulin resistance based on HOMA-IR. The C18:0/C16:0 ratio was significantly lower and that of the C18:1n9/C18:0 ratio was significantly higher in the group with insulin resistance ($p < 0.01$ and $p = 0.01$, respectively) (Fig. 1A), whereas no significant difference was noted in the C16:1n7/C16:0 ratio between the groups. Similarly, when patients were divided into two groups with (≦0.33) and without (>0.33) insulin resistance based on the QUICKI, the C18:0/C16:0 ratio was significantly lower and the C18:1n9/C18:0 ratio was significantly higher in the group with insulin

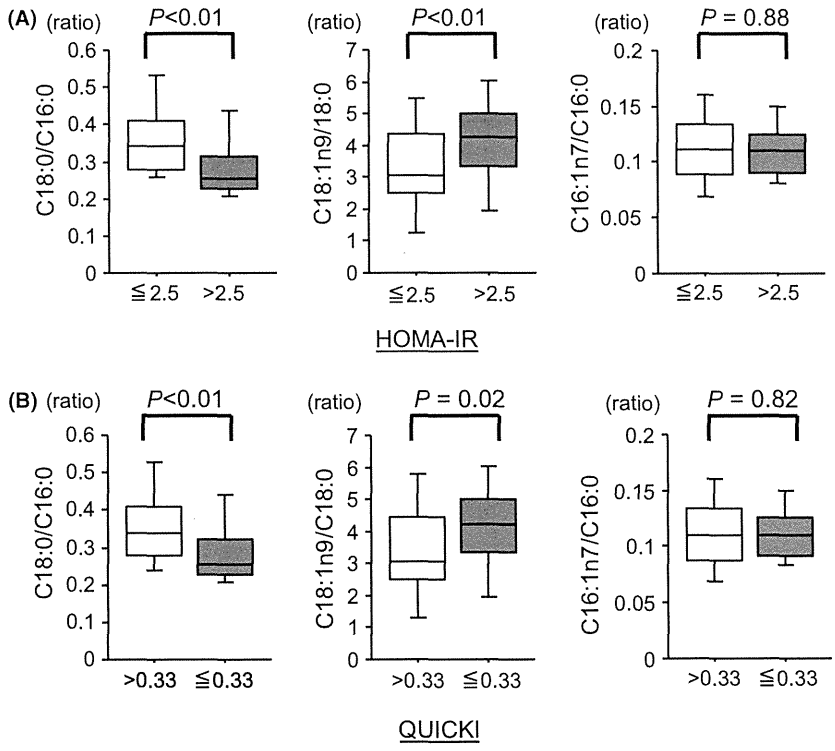

Fig. 1. Association between insulin resistance and the fatty acid composition ratio in liver tissue. The association between insulin resistance and changes in the fatty acid composition ratio in liver tissue was analysed using the Mann–Whitney *U*-test. (A) Patients were divided into groups with and without insulin resistance based on the Homoeostasis Model Assessment for insulin resistance (HOMA-IR) >2.5 as insulin-resistant. (B) Patients were divided into groups with and without insulin resistance based on the QUICKI <0.33 as insulin-resistant.

resistance ($P < 0.01$ and $P = 0.02$, respectively) (Fig. 1B), whereas the C16:1n7/C16:0 ratio showed no association with the presence or absence of insulin resistance.

Fatty acid composition ratio and histopathological findings of the liver

The histopathological findings of the liver with NAFLD were evaluated based on four evaluation items (three items of NAS: steatosis, lobular inflammation, hepatocellular ballooning, and liver fibrosis), and their associations with the liver tissue fatty acid composition ratio were investigated. On evaluation of the association between the NAS and fatty acid composition ratio, the C18:0/C16:0 ratio was significantly lower ($P < 0.01$) and the C18:1n9/C18:0 and C16:1n7/C16:0 ratios were significantly higher ($P < 0.01$) in the group with a 4 or lower score than in the group with a 5 or higher score, showing differences similar to those between the SS and NASH groups (Fig. 2A). Regarding fatty changes (steatosis score), various fatty acid contents significantly increased with an increase in the score. A significant decrease in the C18:0/C16:0 ratio ($P < 0.01$) and a significant increase in the C18:1n9/C18:0 ratio ($P < 0.01$) were noted in the fatty acid composition, but no association with the C16:1n7/C16:0 ratio was noted (Fig. 2B). Regarding lobular inflammation, the C18:0/C16:0 ratio significantly decreased ($P = 0.04$) and the C16:1n7/C16:0 ratio significantly increased ($P < 0.01$) with an increase in the score (Fig. 2C). Regarding hepatocellular ballooning, the C18:0/C16:0 ratio significantly decreased ($P < 0.01$) and the C16:1n7/C16:0 ratio significantly increased ($P < 0.01$) with an increase in the score (Fig. 2D). Similarly, the C18:0/C16:0 ratio significantly decreased ($P < 0.01$) and the C16:1n7/C16:0 ratio significantly increased ($P < 0.01$) with an increase in the fibrosis score (Fig. 2E).

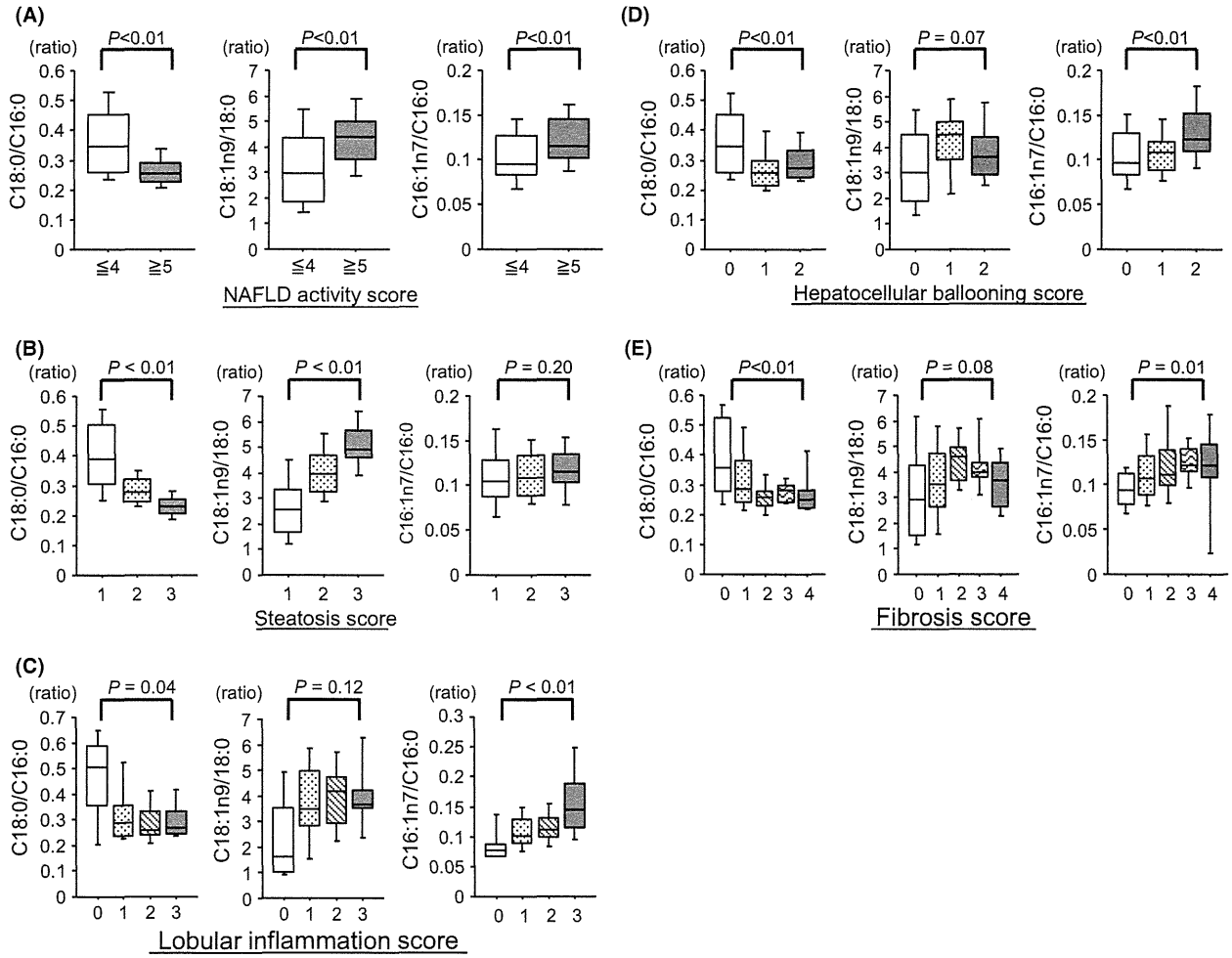

Fig. 2. Relationship between the histopathological findings of the liver and fatty acid composition ratio. The association between the histopathological findings of the liver and fatty acid composition ratio was evaluated using the Spearman's rank correlation coefficient. (A) NAS, (B) steatosis score, (C) lobular inflammation score, (D) hepatocellular ballooning score and (E) fibrosis score.

Expression of fatty acid metabolism-related genes

The gene expression levels of enzymes involved in fatty acid metabolism in liver tissue were investigated. Samples of 65 (SS: 35, NASH: 30) patients were subjected to RTD-PCR, and the gene expression levels of seven enzymes: SCD1, ELOVL6, fatty acid synthase (FAS), sterol regulatory element-binding protein-1c (SREBP-1c), acetyl-CoA carboxylase (ACC), peroxisome proliferator-activated receptor-α (PPARα) and PPARγ were measured. The expression levels of SCD1, ELOVL6, SREBP-1c, FAS and PPARγ were significantly higher in the NASH group than in the SS group, which confirms that the gene expression levels of enzymes involved in fatty acid metabolism were markedly different between the SS and NASH groups (Fig. 3). Thus, the associations between the gene expression levels of these enzymes and histopathological findings (steatosis, inflammation, hepatocellular ballooning and liver fibrosis) were investigated. No significant correlation was noted between the steatosis score and the expression of the fatty acid metabolism-related genes (Fig. 4A); however, a significant correlation was observed between the lobular inflammation score and SCD1 expression ($P < 0.01$), and the gene expression level rose as inflammation progressed in liver tissue (Fig. 4B). The hepatocellular ballooning score was also significantly correlated with the individual gene expression levels of SCD1, ELOVL6, SREBP-1c, FAS, ACC and PPARγ, and expression levels increased as the score rose (Fig. 4C). The fibrosis score was correlated with SREBP-1c expression, but no significant correlation with any other related genes was noted (Fig. 4D).

Finally, we performed a multiple linear regression analysis to calculate age-, sex- and BMI-adjusted coefficients between the histological scores of the liver and experimental parameters such as fatty acid composition, insulin resistance and gene expression (Table 4). In univariate analysis, the steatosis score was significantly correlated with C18:0/C16:0, C18:1n9/C18:0 and QUICKI. In multivariate analysis using these parameters, C18:0/C16:0 was the factor most associated with the steatosis score. In contrast, the inflammation score was significantly correlated with C16:1n7/C16:0, C18:0/C16:0, C18:1n9/C18:0 and SCD1 in univariate analysis and C16:1n7/C16:0 was identified to be the factor most associated with the score in multivariate analysis. The ballooning score was significantly correlated with multiple factors as shown in Table 4 and QUICKI was significantly correlated in multivariate analysis. The fibrosis score was significantly correlated with C18:0/C16:0 only.

Discussion

There have been several reports on fatty acid accumulation in liver tissue in NAFLD. Myristic acid (C14:0), palmitic acid (C16:0) and oleic acid (C18:0) were increased in NAFLD liver tissue in a mouse model (19), and decreases in γ-linolenic acid (C18:3n6) and arachidonic acid (20:4n6) and an increase in the ratios of n-6 and n-3 fatty acids were observed in humans, although the number of cases was small (14). Similar to these findings, the various fatty acid contents of liver tissue were increased in our NAFLD patients. In addition to these fatty acid contents, we closely investigated the fatty acid composition ratios and fatty acid-metabolizing enzymes in the liver tissue in the SS and NASH groups. Regarding the fatty acid composition ratio, significant differences were noted in the C18:0/C16:0, C18:1n9/C18:0 and C16:1n7/C16:0 ratios between the SS and NASH groups, which confirms that the composition ratio of fatty acids is closely associated with the

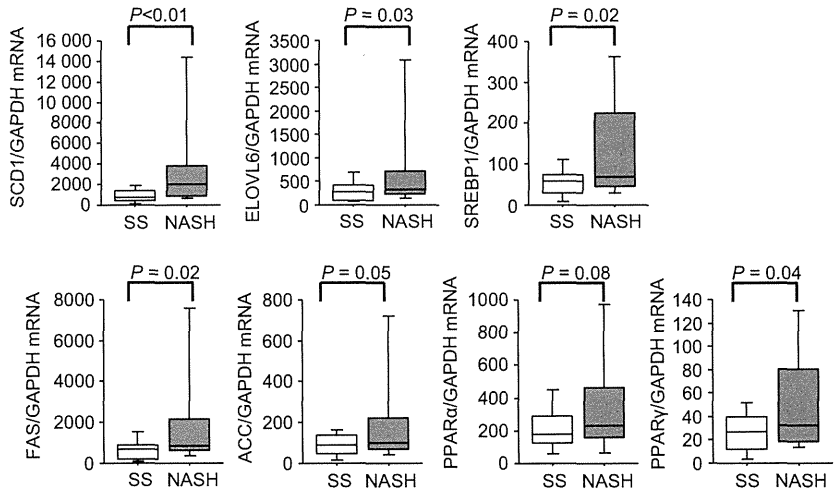

Fig. 3. Expression of fatty acid metabolism-related genes in liver tissue. In 65 patients (SS: 35, NASH: 30), the expression levels of fatty acid metabolism-related genes were measured using RT-PCR, and evaluated using the Mann–Whitney *U*-test.